Beyond near infrared lossy mode resonances with fluoride glass optical fiber

I. VITORIA[1,2], C. R. ZAMARREÑO[1,2*], A. OZCARIZ[1], J. J. IMAS[1,2], I. R. MATIAS[1,2]

[1] *Electrical, Electronic and Communications Engineering Department, Public University of Navarra, 31006 Pamplona, Spain*
[2] *Institute of Smart Cities (ISC), Public University of Navarra, 31006 Pamplona, Spain*
**Corresponding author: carlos.ruiz@unavarra.es*

Received XX Month XXXX; revised XX Month, XXXX; accepted XX Month XXXX; posted XX Month XXXX (Doc. ID XXXXX); published XX Month XXXX

The objective of this work consists of the exploration of the lossy mode resonance (LMR) phenomenon beyond the near infrared region and specifically in the short and medium wave infrared region (SWIR and MWIR). The experimental and theoretical results show for the first time not only LMRs in these regions but also the utilization of fluoride glass optical fiber associated to this phenomenon. Fabricated devices consist of a nanometric thin-film of titanium dioxide (TiO_2) used as LMR generating material, which probed extraordinary sensitivities to external refractive index (RI) variations. RI sensitivity was studied in SWIR and MWIR under different conditions, such as LMR wavelength range or the order of resonance, showing a tremendous potential for the detection of minute concentrations of gaseous or biological compounds in different media.

Optical fiber sensors based on the Lossy Mode Resonance (LMR) phenomenon have been studied and gained popularity in the recent years [1]. The combination of the advantages of the optical fiber sensors (sensing in remote places, resistance to rough environments, etc. [2]) and the use of non-metallic sensing materials in the fabrication of nanometric thin-films (polymers[3] and metal oxides [4]) enable promising sensors in fields such as biosensing [5] or industry for detection of gases and chemicals [6], for instance. The LMR phenomenon is categorized in the group of resonance optical sensors with others such as Surface Plasmon Resonance (SPR) [7] or Localized Surface Plasmon Resonance (LSPR) [8]. In these cases, maximum attenuation peaks, known as resonances, are obtained as a function of the properties of the material surrounding the optical waveguide (in this case, optical fiber). Changes in the optical properties of the material surrounding the optical waveguide or in the refractive index (RI) of the surrounding medium cause a resonance wavelength shift, which can be exploited for sensing purposes [1]. The distinctive characteristics of the LMR phenomenon (high sensitivity, wide range of coating materials, etc. [1]) make it optimal for the development of fiber sensors. Till date, a wide variety of LMR sensors have been developed in the visible (VIS) [9,10] and near infrared (NIR) [11,12] regions, being VIS and NIR regions approx. between 400-900 nm and 900-1700 nm respectively. Here, it must be taken into account that the limits of the regions are not well defined, so the borders could be slightly changed depending on the sources. VIS LMR sensors are more popular, which can be associated to the reduced cost of the equipment in this region, while NIR LMR sensors are used for the most demanding applications. NIR LMR sensors are generally used due to the requirement of high sensitivities, which is increased for LMRs located at longer wavelengths. Here, it is interesting to consider the possibility to use optical fiber and optical communications standard equipment in first, second or third communication windows in order to reduce the application cost. However, higher sensitivities still require to work at longer wavelengths outside standard optical communications. This wavelength range, known as mid infrared region (MIR) is still unknown in the LMR sensors field. MIR, as many other regions of the electromagnetic spectrum, has diffusive borders but can be roughly considered to be in the range between 2 μm and 20 μm [13]. A more precise differentiation of MIR can be found in other works that divide this region further in several bands: short, wave infrared (SWIR), medium wave infrared (MWIR) and long wave infrared (LWIR) located approximately between 1-2.5 μm, 3-5 μm and 8-12 μm respectively. One of the main advantages of the MIR region is the valuable information that can be extracted in this band from the characteristic absorption peaks associated to the different gaseous and chemical compounds [14]. These characteristic absorption peaks are generated by the vibration of the molecules that produces sharp and distinctive peaks for different organic and inorganic compounds. On the other hand, the cost of the detection equipment used for the detection in the MIR region is considerably higher than that used in the VIS or NIR region, which could be associated to the fact that this region of the spectrum is less developed and popular. In addition, the width of the region (1-12 μm) makes it difficult to find technologies and materials suitable to cover the whole spectral region. For example, conventional silica optical fibers do not transmit in the MIR region, as the attenuation starts to greatly increase at wavelengths above 1800 nm [15]. For these applications, fluoride glass fibers that have a transmission window between 0.3-4.5 μm, are used [16,17]. These optical fibers have been deeply studied due to the extraordinary theoretical low attenuation of 0.01dB/Km[17] with plenty of applications in communications, where the number of repeaters can significantly be reduced. Moreover, fluoride optical

fibers find other niche applications where the fibers allow to efficiently transmit the infrared light, such as in remote infrared spectroscopy [18] or high power laser fabrication [19].

The aim of this work consists of studying the LMR phenomenon and its sensitivity in the MIR region using fluoride glass optical fibers. To the best knowledge of the authors, this is the first time that LMRs are shown in the MIR region and it will be also the first time that LMRs are obtained using a fluoride glass optical fiber. In particular, the study and characterization of the LMR phenomenon will be done experimentally and compared with simulated theoretical results that will help us to extract further conclusions beyond the experimental results.

Several devices were fabricated and analyzed for the experimental part of this study. These devices are modified fluoride glass multimode optical fibers, in which a segment of 1 cm was uncladded and coated with a nanometric thin-film of titanium dioxide (TiO_2). Fluoride glass optical fibers with a diameter of 250/290 µm core/cladding and numeral aperture >0.4 were purchased from Le Verre Fluoré. The core is made of Zirconium ZrF4 Fluoride Glass (ZFG) with a RI between 1.51 and 1.49 (in the studied region of this work) and the cladding is made of a low index resin. The cladding was chemically removed using a stripping gel provided by the fiber manufacturer as it can been seen in the image close up of Fig 1. Decladded fibers were coated with TiO_2 by means of the atomic layer deposition (ALD) technique using a Savannah G2 ALD System (Veeco) at a temperature of 100 ºC in vacuum with a N2 flow rate of 90 sccm. The chemical precursors used in this process were deionized water (DI H_2O) and TDMAT (Tetrakis (dimethylamido)titanium(IV)). The optical fiber interrogation setup consisted of a typical transmission configuration (see Fig. 1), composed by a Takhi halogen lamp from Pyroistech, and a combination of different spectrometers depending on the region of the spectrum studied. The spectrometers used were HR4000 (in the range 200-1100 nm) and NirQuest (in the range 900-1700 nm) from Ocean Optics and ANIR FT-NIR spectrometer (in the range 900-2600 nm) from Arcoptix to study the VIS, NIR and SWIR respectively.

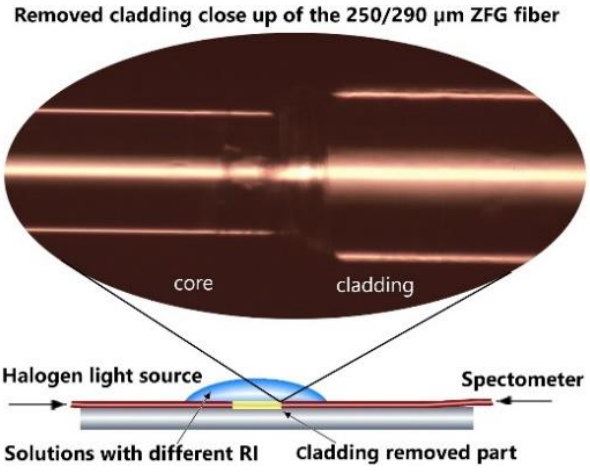

Fig. 1. Sensor setup in a transmission configuration where different RI solutions surround the sensitive part of the optical fiber.

During the study of the sensor, the sensitive region of the fiber was covered with a few drops of water-glycerol solutions with different RI (see Fig. 1). All the tests were performed at room temperature (25ºC). The RI of the solutions was measured using the handheld refractometer Refracto 30GS from METTLER TOLEDO. Here it has to be taken into account the RI value given by the instrument corresponds to the wavelength of 590 nm and this value can be slightly different at larger wavelengths, which is the case of our study. In this sense, RI data for H_20 tabulated at different wavelengths is obtained from previous study [20]. The Cauchy formula is implemented [21] in order to estimate the RI of glycerol in the SWIR. Therefore, the RI of the mixed water/glycerol solutions in the SWIR can be obtained by combining both approximations proportionally to the concentrations of the mix, from the RI measurements performed in the VIS.

Theoretical results permitted to extract the fabrication parameters for the experimental test, such as the nanometric thin-film thickness for the observation of the LMR in the SWIR range. The theoretical curves have been calculated by means of a numerical analysis based on the well-known plane wave method for a one-dimensional multilayer waveguide [22] and validated for LMRs [23]. The values used for the RI of the fiber core have been provided in the range from 0.5 µm to 4.5 µm by the manufacturer of the fiber. The RI of the TiO_2 nanometric thin-film was obtained experimentally using spectroscopic ellipsometry measurements using a UVISEL 2 ellipsometer (Horiba Ltd).

A study of the correlation between the resonance positions and the thickness of the films is performed in order to verify and compare the simulation results with the experimental data. Several probes were fabricated for this purpose with different TiO_2 thin-film thicknesses. The transmission spectra of each probes was studied using the setup shown in Fig. 1. The resonance wavelength position was obtained using a simple MATLAB™ algorithm that models the peaks of the resonances using parabola curves. This technique produces more accurate data due to the smoothing of the curves and the removal of the noise as well as enable a systematic determination of the LMR central wavelength. Resonance wavelengths are represented as a function of the thickness in Fig. 2. Here, all the experimental data (points) of the graph were acquired in the same conditions of temperature and humidity and using the air as the surrounding medium of the fiber.

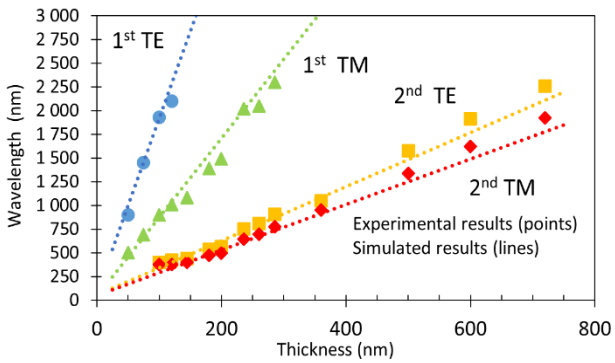

Fig. 2. Correlation between the nanofilm thickness and the resonance wavelength positions with experimental and simulated data.

Here, it is important to note that two resonance peaks can be differentiated for each LMR order, corresponding to the TE (transverse electric) and TM (transverse magnetic) components [24]. For the sake of clarity, only the first and second LMRs are displayed in the graph. Higher order LMRs could also be obtained increasing the thickness of the thin-film but with lower sensitivities [23], being less attractive to be used in sensing applications. As it can be seen in Fig. 2, the resonances shift to longer wavelengths with the increase of the film's thickness. Also, the slope of each peak is different, being higher the one of the resonances that first appear. In particular, TE component has a slope greater than the TM. Moreover, low order resonances move faster than high order resonances. Due to this behaviour, the resonances separate from each other as they shift to longer wavelengths of the spectrum or, in other words, as a function of the film thickness. Another characteristic showed in the experimental data and corroborated with the simulations is the fact that the first order LMR is wider (since the 1st order LMR depth is less than 3dB, which is the standard for FWHM parameter, it is required to use an analogy redefining the width in this case, as the spectral distance marked by the points in the curve 1 dB below the LMR peak) than higher order LMRs. Particularly, the TM component of the first order LMR has a width of 113 nm (at 689 nm in air and 75 nm thickness probe) while second order LMRs are sharper with a width of 36 nm for the TM component (at 695 nm in air and 260 nm thickness probe).

Apart from the previously reviewed connection between the thickness of the thin-film and the resonance wavelength position there is another important performance parameter associated to these devices, the sensitivity to the external medium. In order to study this parameter, the sensitive region of the devices is submerged in different RI solutions as it was indicated before. From previous studies [23], first order LMRs have the greatest sensitivity. However, the low depth and large width of their absorption peaks make it difficult in some cases the determination of the resonance wavelength position with high accuracy. For that reason, the second LMR will be selected for this study as it has been also pointed out in previous works [25]. In Fig. 3, the absorbance spectrum of the sensor is showed in the VIS, NIR and SWIR with water (RI=1.3334) and air (RI=1) as the outer media. Resonances of different orders from the 2nd to the 8th can be also observed in Fig. 3. Moreover, it can be also appreciated in Fig. 3 the decreasing sensitivities for higher order resonances, which present smaller resonance shifts between the air and water.

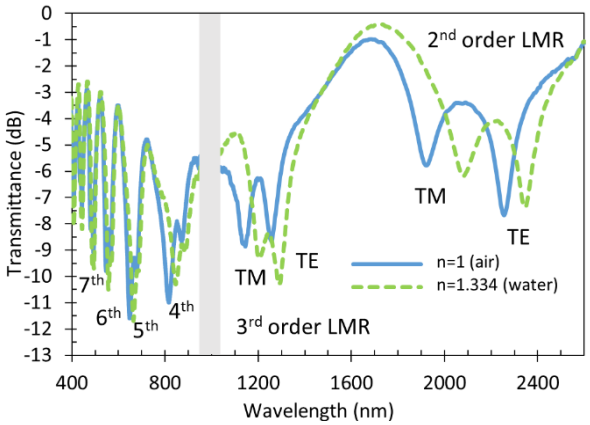

Fig. 3. Transmittance spectra of the 720 nm thickness probe when the sensitive region is submerged in water and air.

In Fig. 4 it is presented a detailed study of the second order resonance in the SWIR. Here, the sensitive region of the device is submerged in solutions with different RI. Both TE (right) and TM (left) components of the second order LMR can be observed for different outer medium RI. An increase of the RI shifts both resonances, TE and TM components, to longer wavelengths. In spite of TE component location at larger wavelengths th, TM component shift is larger than that of TE component, which is associated to the fact that the TM component sensitivity to RI variations is higher than that of the TE component. This effect is better illustrated in the sensitivity curves shown in the inset of Fig. 4. Here, the sensitivities represented in the inset have been calculated as the wavelength shift in nanometers divided by the refractive index units (RIU) variation that induces this shift. In particular, the sensitivity is 1,797.2 nm/RIU for the TM component and 836.8 nm/RIU for TE component for a change of RI from 1.4001 to 1.4325. Furthermore, experimental data represented in Figs. 2 and 4 corroborate the simulations, demonstrating the reliability of the theoretical models and their similarity with the experimental data.

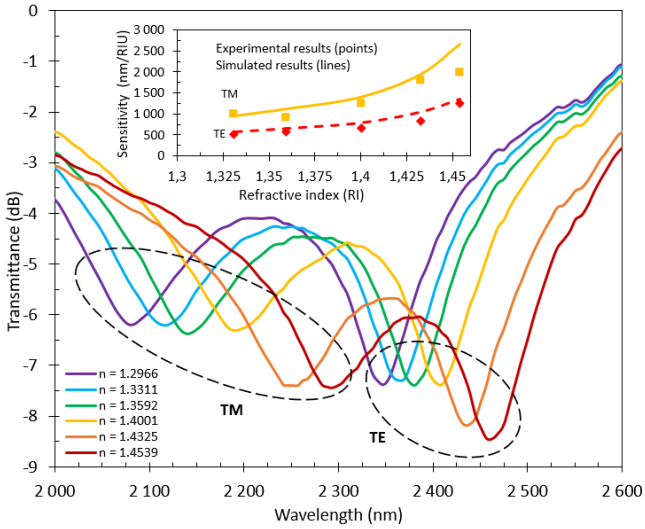

Fig. 4. Transmittance spectra of the second order LMR (SWIR) when the sensitive region is submerged in different RI solutions. Inset: Sensitivity (experimental and theoretical) of TE and TM components of the 2nd LMR.

First order LMR sensitivity has been theoretically obtained applying the initially described and later experimentally corroborated simulation techniques. Obtained simulations revealed a sensitivity of the first order LMR (TM component) of 12,083 nm/RIU in a RI range between 1.4001 and 1.4325 at a wavelength of 2,250 nm, which implies an increase factor of 6.72 compared to the TM component of the second order resonance in the same conditions. However, the large width and low absorbance of the first LMR, as it was mentioned earlier, would require the utilization of polarized light or more specific optical waveguides in order to exploit the benefits of its high sensitivity for practical sensing applications.

An additional simulation is presented in Fig. 5 in order to analyze the increase of sensitivity of the 2nd order resonance in the MWIR region. In this simulation, a linear growth of the sensitivity is found

when the LMR is observed at longer wavelengths. The sensitivity has been calculated with water as the surrounding medium, more specifically a RI change between 1.33 and 1.34.

The experimental study in this work has been performed only until 2.5 μm because of the limitations of the spectrometer, showing good agreement between experimental and theoretical studies within that range. The utilization of equipment at longer wavelengths could also be used to corroborate theoretical simulations in the MWIR that reveal extremely sensitive devices in that range as it can be seen in Fig. 5. It is difficult to make a fair comparison between current device and previous works that use different optical fiber, materials or wavelength working range. Thus, obtained devices have been compared under the same conditions showing that the sensitivity increases by a factor of 9.89 when the LMR shifts from 1,000 to 5,000 nm due to a variation in coating thickness.

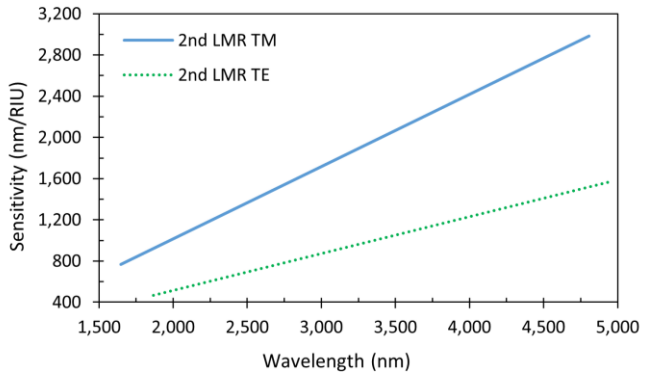

Fig. 5. Sensitivity of the second LMR (SWIR-MWIR). Theoretical results.

The experimental results of the LMR effect in the SWIR region have proven for the first time the feasibility for the fabrication of a LMR-based device in this region as well as, establishing a record for the longest LMR wavelength observed experimentally until now (2,500 nm). Moreover, it has been experimentally demonstrated the observation of LMR in the SWIR (1.7-2.5 μm) and theoretically in the SWIR-MWIR (1.7-5 μm) regions. This work has also reported for the first time the utilization of a fluoride glass optical fiber for LMR generation, opening new frontiers for the development of novel LMR-based devices with high sensitivity in the MIR. The simulated results have been corroborated with experimental data, showing that the LMR effect theoretically continues and increases the sensitivity in longer wavelengths (MWIR).

Finally, it is important to remark that this work consist of a first approach for the establishment of LMR-based sensors as versatile tools for sensing in the MIR region. The results presented here could open the door to a great number of possibilities due to the unique properties and large range of the MIR region. The sensing mechanisms studied in this paper could be also further developed by means of the utilization of more sophisticated optical waveguides, the combination of different thin-film materials or the utilization of analyte-specific overlays that enable to obtain sharper resonances, as well as improve the performance of the devices for sensing purposes.

Funding. Ministerio de Ciencia, Innovación y Universidades (FPU18/03087); Agencia Estatal de Investigación (PID2019-106231RB-I00 TEC).

References

1. I. Del Villar, F. J. Arregui, C. R. Zamarreño, J. M. Corres, C. Bariain, J. Goicoechea, C. Elosua, M. Hernaez, P. J. Rivero, A. B. Socorro, A. Urrutia, P. Sanchez, P. Zubiate, D. Lopez, N. De Acha, J. Ascorbe, and I. R. Matias, Sensors Actuators, B Chem. **240**, 174 (2017).
2. D. Pawar and S. N. Kale, Microchim. Acta **186**, (2019).
3. C. R. Zamarreño, M. Hernáez, I. Del Villar, I. R. Matías, and F. J. Arregui, Sensors Actuators, B Chem. **155**, 290 (2011).
4. S. P. Usha, A. M. Shrivastav, and B. D. Gupta, Opt. Fiber Technol. **45**, 146 (2018).
5. P. Zubiate, A. Urrutia, C. R. Zamarreño, J. Egea-Urra, J. Fernández-Irigoyen, A. Giannetti, F. Baldini, S. Díaz, I. R. Matias, F. J. Arregui, E. Santamaría, F. Chiavaioli, and I. Del Villar, Biosens. Bioelectron. X **2**, 100026 (2019).
6. I. Vitoria, C. R. Zamarreño, A. Ozcariz, and I. R. Matias, Sensors (Switzerland) **21**, 1 (2021).
7. B. D. Gupta and R. Kant, Opt. Laser Technol. **101**, 144 (2018).
8. K. M. Mayer and J. H. Hafner, Chem. Rev. **111**, 3828 (2011).
9. S. P. Usha, S. K. Mishra, and B. D. Gupta, Sensors Actuators, B Chem. **218**, 196 (2015).
10. D. Tiwari, K. Mullaney, S. Korposh, S. W. James, S. W. Lee, and R. P. Tatam, Sensors Actuators, B Chem. **242**, 645 (2017).
11. F. J. Arregui, I. Del Villar, C. R. Zamarreño, P. Zubiate, and I. R. Matias, Sensors Actuators, B Chem. **232**, 660 (2016).
12. P. Zubiate, C. R. Zamarreño, P. Sánchez, I. R. Matias, and F. J. Arregui, Biosens. Bioelectron. **93**, 176 (2017).
13. D. Popa and F. Udrea, Sensors (Switzerland) **19**, 1 (2019).
14. Y. Wang, K. Zheng, F. Song, F. K. Tittel, and C. Zheng, 2020 5th Optoelectron. Glob. Conf. OGC 2020 80 (2020).
15. M. T. Harrison, S. V. Kershaw, M. G. Burt, A. L. Rogach, A. Kornowski, A. Eychmüller, H. Weller, and A. L. Rogach, Pure Appl. Chem. **72**, 295 (2000).
16. I. D. Aggarwal and G. Lu, (Elsevier Science, 2013).
17. M. Saad, Fiber Opt. Sensors Appl. VI **7316**, 73160N (2009).
18. S. J. Saggese, M. R. Shahriari, and G. H. Sigel Jr, in *Infrared Optical Materials IV* (International Society for Optics and Photonics, 1988), **929**, pp. 106–114.
19. X. Zhu and N. Peyghambarian, Adv. Optoelectron. **2010**, (2010).
20. G. M. Hale and M. R. Querry, Appl. Opt. **12**, 555 (1973).
21. P. R. Cooper, Appl. Opt. **22**, 3070 (1983).
22. R. Ota, S. Seki, M. Ogawa, T. Nishide, A. Shida, M. Ide, and Y. Sawada, in *Thin Solid Films* (Elsevier, 2002), **411**, pp. 42–45.
23. I. Del Villar, M. Hernaez, C. R. Zamarreno, P. Sánchez, C. Fernández-Valdivielso, F. J. Arregui, and I. R. Matias, Appl. Opt. **51**, 4298 (2012).
24. C. Ruiz Zamarreño, P. Zubiate, M. Sagües, I. R. Matias, and F. J. Arregui, Opt. Lett. **38**, 2481 (2013).
25. A. Ozcariz, D. A. Piña-Azamar, C. R. Zamarreño, R. Dominguez, and F. J. Arregui, Sensors Actuators, B Chem. **281**, 698 (2019).

1. I. Del Villar et al., "Optical sensors based on lossy-mode resonances," Sensors Actuators, B Chem. 240, 174–185 (2017).
2. D. Pawar and S. N. Kale, "A review on nanomaterial-modified optical fiber sensors for gases, vapors and ions," Microchim. Acta 186, (2019).
3. C. R. Zamarreño et al., "Optical fiber pH sensor based on lossy-mode resonances by means of thin polymeric coatings," Sensors Actuators, B Chem. 155, 290–297 (2011).
4. S. P. Usha, A. M. Shrivastav, and B. D. Gupta, "Semiconductor metal oxide/polymer based fiber optic lossy mode resonance sensors: A contemporary study," Opt. Fiber Technol. 45, 146–166 (2018).
5. P. Zubiate, A. Urrutia, C. R. Zamarreño et al., "Fiber-based early diagnosis of venous thromboembolic disease by label-free D-dimer detection," Biosens. Bioelectron. X 2, 100026 (2019).
6. I. Vitoria, C. R. Zamarreño, A. Ozcariz, and I. R. Matias, "Fiber optic gas sensors based on lossy mode resonances and sensing materials used therefor: A comprehensive review," Sensors MDPI 21, 1–26 (2021).
7. B. D. Gupta and R. Kant, "Recent advances in surface plasmon resonance based fiber optic chemical and biosensors utilizing bulk and nanostructures," Opt. Laser Technol. 101, 144–161 (2018).
8. K. M. Mayer and J. H. Hafner, "Localized surface plasmon resonance sensors," Chem. Rev. 111, 3828–3857 (2011).
9. S. P. Usha, S. K. Mishra, and B. D. Gupta, "Fiber optic hydrogen sulfide gas sensors utilizing ZnO thin film/ZnO nanoparticles: A comparison of surface plasmon resonance and lossy mode resonance," Sensors Actuators, B Chem. 218, 196–204 (2015).
10. D. Tiwari, K. Mullaney, S. Korposh, S. W. James, S. W. Lee, and R. P. Tatam, "An ammonia sensor based on Lossy Mode Resonances on a tapered optical fibre coated with porphyrin-incorporated titanium dioxide," Sensors Actuators, B Chem. 242, 645–652 (2017).
11. F. J. Arregui, I. Del Villar, C. R. Zamarreño, P. Zubiate, and I. R. Matias, "Giant sensitivity of optical fiber sensors by means of lossy mode resonance," Sensors Actuators, B Chem. 232, 660–665 (2016).
12. P. Zubiate, C. R. Zamarreño, P. Sánchez, I. R. Matias, and F. J. Arregui, "High sensitive and selective C-reactive protein detection by means of lossy mode resonance based optical fiber devices," Biosens. Bioelectron. 93, 176–181 (2017).
13. D. Popa and F. Udrea, "Towards integrated mid-infrared gas sensors," Sensors MDPI 19, 1–15 (2019).
14. Y. Wang, K. Zheng, F. Song, F. K. Tittel, and C. Zheng, "Mid-Infrared Absorption Spectroscopy for Gas Sensing and Application," 2020 5th Optoelectron. Glob. Conf. OGC 2020 80–82 (2020).
15. M. T. Harrison, S. V. Kershaw, M. G. Burt, et al., "Colloidal nanocrystals for telecommunications. Complete coverage of the low-loss fiber windows by mercury telluride quantum dot," Pure Appl. Chem. 72, 295–307 (2000).
16. I. D. Aggarwal and G. Lu, Fluoride Glass Fiber Optics (Elsevier Science, 2013).
17. M. Saad, "Fluoride glass fiber: state of the art," Fiber Opt. Sensors Appl. VI 7316, 73160N (2009).
18. S. J. Saggese, M. R. Shahriari, and G. H. Sigel Jr, "Fluoride fibers for remote chemical sensing," in Infrared Optical Materials IV (International Society for Optics and Photonics, 1988), 929, pp. 106–114.
19. X. Zhu and N. Peyghambarian, "High-power ZBLAN glass fiber lasers: Review and prospect," Adv. Optoelectron. 2010, (2010).
20. G. M. Hale and M. R. Querry, "Optical Constants of Water in the 200-nm to 200-µm Wavelength Region," Appl. Opt. 12, 555 (1973).
21. P. R. Cooper, "Refractive-Index measurements of liquids used in conjunction with optical fibers," Appl. Opt. 22, 3070 (1983).
22. R. Ota et al., "Fabrication of indium-tin-oxide films by dip coating process using ethanol solution of chlorides and surfactants," in Thin Solid Films, 411, pp. 42–45.
23. I. Del Villar, M. Hernaez, C. R. Zamarreno, P. Sánchez, C. Fernández-Valdivielso, F. J. Arregui, and I. R. Matias, "Design rules for lossy mode resonance based sensors," Appl. Opt. 51, 4298–4307 (2012).
24. C. Ruiz Zamarreño, P. Zubiate, M. Sagües, I. R. Matias, and F. J. Arregui, "Experimental demonstration of lossy mode resonance generation for transverse-magnetic and transverse-electric polarizations," Opt. Lett. 38, 2481 (2013).
25. A. Ozcariz, D. A. Piña-Azamar, C. R. Zamarreño, R. Dominguez, and F. J. Arregui, "Aluminum doped zinc oxide (AZO) coated optical fiber LMR refractometers—An experimental demonstration," Sensors Actuators, B Chem. 281, 698–704 (2019).